Transonic Flow Around Airfoils with Relaxation and Energy Supply by Homogeneous Condensation

Günter H. Schnerr* and Ulrich Dohrmann†
University of Karlsruhe, Karlsruhe, Federal Republic of Germany

Steady two-dimensional flow of vapor/carrier gas mixtures (moist air) with nonequilibrium condensation is investigated in theory and experiment. Aside from Laval nozzles, transonic flow over airfoils at $M_\infty \lesssim 1$ is considered. The numerical calculation is based on the Euler equation linked with the classical theory of homogeneous nucleation and droplet growth using a new diabatic, time-dependent, explicit, finite volume method. By means of this model, the effects of energy supply in local supersonic flow over airfoils are investigated including a detailed analysis of the two-dimensional structure in the diabatic case. The variation of the pressure drag coefficient due to the heating is the sum of the following connected processes: the reduction of the wave drag in the local supersonic area producing a higher Mach number behind the shock, the shock shifting, and the pressure increase in the rear section of an airfoil due to evaporation. Both airfoil series investigated, circular arc and NACA-0012, show the same tendency concerning the shifting of the normal shock. But the pressure drag coefficients vary in opposite directions with different supply conditions.

Nomenclature

c	= airfoil chord length
c_D	= pressure drag coefficient
c_p	= pressure coefficient
g	= mass fraction of condensate (sublimate)
h	= enthalpy
J	= nucleation rate
k	= Boltzmann constant
L	= latent heat
m	= mass per molecule—water
M_∞	= test section reference Mach number
$M_{f,\infty}$	= frozen freestream Mach number
n^*	= number of molecules of a critical nucleus
p	= static pressure
$p_{s,r}$	= saturation pressure of droplet with radius r
$p_{s,\infty}$	= saturation pressure of a plane liquid surface
Q_0	= $\sim\Sigma$ of droplets per unit mass
Q_1	= $\sim\Sigma$ of droplet radii per unit mass
Q_2	= $\sim\Sigma$ of droplet surfaces per unit mass
r	= droplet radius
$\bar{r}$	= surface averaged droplet radius, $\bar{r}=\sqrt{Q_2/Q_0}$
r^*	= critical droplet radius
R_v	= specific gas constant of water vapor
R^*	= radius of curvature at the nozzle throat
s	= supersaturation ratio
t	= time, thickness parameter
T	= temperature
u	= velocity component in x direction
v	= velocity component in y direction
x	= Cartesian coordinate; mixing ratio
y	= Cartesian coordinate
α	= condensation coefficient
Φ	= relative humidity
ρ	= density
σ_∞	= surface tension of a plane surface

Subscripts and Superscripts

ad	= adiabatic flow
c	= condensate (sublimate), condensation onset
d	= diabatic flow
f	= frozen
v	= vapor
q	= heat addition
s	= saturation
0	= stagnation condition
1	= before heat addition
∞	= freestream; test section reference; plane surface
$*$	= values at $M=1$; values of critical nucleus

Introduction

ENERGY supply in transonic flows by nonequilibrium condensation is of basic interest and useful for technical applications and experimental methods, e.g., turbo machinery, cryogenic wind tunnels or shock tubes. When energy is supplied to the flow by homogeneous condensation of a vapor, the onset, development, and amount of the heat addition is controlled by the flow itself. Flow and heat addition cannot be separated. Changes in the pressure distribution and aerodynamic characteristics of the flow over airfoils that adjust themselves due to the linkage of flow and heat supply are investigated theoretically and experimentally. In fast expansions typical for transonic flows, the vapor component supersaturates after passing the vapor pressure curve. Typical values of the supersaturation ratio $s=p_v(T)/p_{s,\infty}(T)$ for water vapor in a carrier gas in our range are 50–100. The corresponding adiabatic supercooling is about 50 K.[1] It follows that the condensation onset is only possible for $M>1$.[2] This happens in the supersonic part of a nozzle and in the local supersonic region over airfoils. In special cases homogeneous condensation is also possible in the wake of airfoils. Several details are of particular interest to aerodynamicists, the condensation onset (especially on the airfoil), the boundaries of the condensation region, the droplet behavior through the shock, the wake flow, and the variation of the drag and lift coefficients. In this paper the pressure drag is investigated for symmetrical airfoils at zero angle of attack. Zierep and Lin[3] were the first to formulate the similarity law for the Mach number at the condensation onset. The first experimental results concerning transonic flows over airfoils with homogeneous condensation are reported from Head,[4] Schmidt,[5] Hiller

Received April 14, 1989; presented as Paper 89-1834 at the 20th Fluid Dynamics, Plasma Dynamics and Lasers Conference, Buffalo, NY, June 12–14, 1989; revision received Aug. 25, 1989.

*Privatdozent of Fluid Dynamics, Doctor of Engineering Sciences, Institut für Strömungslehre und Strömungsmaschinen, Department of Mechanical Engineering. Senior Member AIAA.

†Graduate Engineer, Institut für Strömungslehre und Strömungsmaschinen, Department of Mechanical Engineering.

and Meier,[6] an extensive description of condensation in steady flows over airfoils is found by Schnerr.[7] Numerical results based on simplified models used for the process of homogeneous condensation were calculated from Robinson, Bauer, and Nichols.[8] A discussion of natural condensation effects in airplane flowfields by Campbell, Chambers and Rumsey[9] can be found. Appropriate results for transonic cascade flows of water vapor are found by Moheban and Young.[10] Relevant—mostly experimental—results for transonic flow in cryogenic wind tunnels are available from Hall,[11,12] Koppenwallner and Dankert,[13] Wagner and Düker,[14] and Wegener.[15,16]

Theory

The conservation equations of mass, momentum, and energy yield

$$\frac{\partial U}{\partial t}+\frac{\partial F}{\partial x}+\frac{\partial G}{\partial y}=Q$$

$$U=\begin{pmatrix}\rho\\ \rho u\\ \rho v\\ \rho e\end{pmatrix}\qquad F=\begin{pmatrix}\rho u\\ \rho u^2+p\\ \rho uv\\ (\rho e+p)u\end{pmatrix}$$

$$G=\begin{pmatrix}\rho v\\ \rho uv\\ \rho v^2+p\\ (\rho e+p)v\end{pmatrix}\qquad Q=\begin{pmatrix}0\\ 0\\ 0\\ \rho\dfrac{\mathrm{d}(Lg)}{\mathrm{d}t}\end{pmatrix} \tag{1}$$

Here e is the total energy per unit mass. The source term in the energy equation denotes the heat supply caused by the condensation process. Air and water vapor are assumed to be perfect gases; the specific heat ratio of moist air is set to $\gamma = 1.4$ (see Ref. 1). In contrast to Ref. 8 homogeneous condensation is here calculated with the classical theory according to Volmer.[17] The nucleation rate per unit time and volume becomes

$$J=\sqrt{\frac{2}{\pi}}\,\sigma_\infty m^{-3/2}\frac{\rho_v^2}{\rho_c}\exp\left(-\frac{\Delta G^*}{kT}\right)$$

$$\Delta G^*=\frac{16}{3}\pi\left(\frac{m}{\rho_c \ell n(s)kT}\right)^2\sigma_\infty^3 \tag{2}$$

Orders typical for the number of molecules in a critical nucleus are $n^* \approx 10$ and for the nucleation rate at the condensation onset $J \approx 10^{22}-10^{24}\ \mathrm{m}^{-3}\mathrm{s}^{-1}$. The dominating property in Eq. (2) is the surface tension σ_∞ appearing in the exponent in the third power. But no definite statements can be made on the nature of the condensate (liquid or solid) at condensation onset temperatures far below the triple point. The surface tension is therefore handled as a free parameter, and calculations are performed assuming both a liquid or solid condensate. The droplet radii in these transonic flows with homogeneous condensation in moist air always remain smaller than the mean free path of the vapor and carrier gas. For this reason the calculation of the droplet growth is based on the Hertz-Knudsen model

$$\frac{\mathrm{d}r}{\mathrm{d}t}=\frac{\alpha}{\rho_c}\frac{p_v-p_{s,r}}{\sqrt{2\pi R_v T}} \tag{3}$$

Here α denotes the condensation coefficient giving the fraction of the rate of molecules that impinge on the drop that stick to it. This coefficient is the second free parameter in the calculation. The condensate mass fraction g in Eq. (1) is defined as the ratio of condensate to total mass of vapor, condensate, and carrier gas. The variation of g is

$$\frac{\mathrm{d}g}{\mathrm{d}t}=\frac{4}{3}\pi\rho_c r^{*3}\frac{J}{\rho}+\int_{-\infty}^{t}\frac{4}{3}\pi\rho_c\frac{J(t)}{\rho(t_1)}\frac{\mathrm{d}r^3(t_1)}{\mathrm{d}t}\,\mathrm{d}t_1 \tag{4}$$

Introducing the surface averaged droplet radius (Hill[18]) and the properties Q_0, Q_1, Q_2, Eq. (4) can be transformed to the following system

$$K=\frac{\partial A}{\partial t}+\frac{\partial B}{\partial x}+\frac{\partial C}{\partial y}$$

$$A=\begin{pmatrix}\rho g\\ \rho Q_2\\ \rho Q_1\\ \rho Q_0\end{pmatrix}\qquad B=\begin{pmatrix}\rho ug\\ \rho uQ_2\\ \rho uQ_1\\ \rho uQ_0\end{pmatrix}\qquad C=\begin{pmatrix}\rho vg\\ \rho vQ_2\\ \rho vQ_1\\ \rho vQ_0\end{pmatrix}$$

$$K=\begin{pmatrix}4\pi\rho_c\left(\dfrac{1}{3}Jr^{*3}+\rho Q_2\dfrac{\mathrm{d}\bar{r}}{\mathrm{d}t}\right)\\ Jr^{*2}+2\rho Q_1\dfrac{\mathrm{d}\bar{r}}{\mathrm{d}t}\\ Jr^{*}+\rho Q_0\dfrac{\mathrm{d}\bar{r}}{\mathrm{d}t}\\ J\end{pmatrix} \tag{5}$$

The two-dimensional diabatic method is a further development of the time-dependent, explicit, finite volume method for adiabatic flows of Eberle.[19] The linked systems of Eqs. (1) and (5) are transformed onto an equidistant mesh. Using flux-extrapolation, second-order accuracy is achieved without any additive dissipation (second-order upwind scheme). A stable solution occurs when the time step for the calculation of the variables ρQ_0, ρQ_1, ρQ_2 and ρg in Eq. (5) is chosen to be 2 orders of magnitude less than for Eq. (1). The grids are generated by a Poisson equation. The maximum number of cells used in Laval nozzles is 182×64. Near the nozzle walls (in normal direction) and at the stagnation points (parallel to the flow direction), the grids are locally concentrated. The O grids with 192×64 cells are used for the airfoil calculations. The distances of the outer calculation boundaries are varied from 10 to 100 airfoil chord lengths.

Analysis of the Numerical Method and Results

Figures 1 and 2 show numerical results of the diabatic flow over a NACA-0012 airfoil with zero angle of attack. In the region of the normal shocks (in the middle of the chord length, $M_{f,\infty} = 0.8$), the enthalpy rises slightly and is quickly reduced. In adiabatic flow, the maximum enthalpy difference $(h_0 - h_{01})/h_{01}$ on the airfoil is equivalent to a heat addition of the latent heat release of about 0.4 g condensate per kg air. In nozzles the corresponding maximum value is about 0.1 g/kg at the walls and one order of magnitude less in the flowfield. As will be shown in the following calculations, these numbers correspond to insignificant errors in the condensation calculations. The contours of constant enthalpy difference of the diabatic flow over the NACA-0012 airfoil are shown in Fig. 1. A level of 0.001 approximately represents the onset of condensation. Downstream of the heat supply the maximum value rises to $(h_0 - h_{01})/h_{01} = 0.013$. In the region right behind the rear stagnation point the condensate evaporates completely. Low negative values (≥ -0.003) of the stagnation enthalpy occur only at the outer boundary of the wake flow. The most

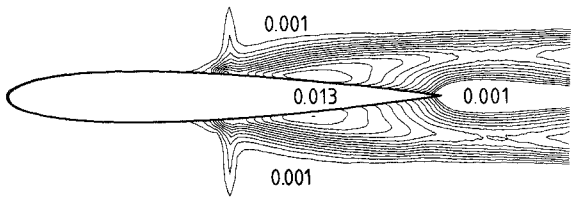

Fig. 1 NACA-0012 airfoil—diabatic flow, $M_{f,\infty} = 0.8$, $\Phi_0 = 30\%$, atmospheric supply, $(h_0 - h_{01})/h_{01}$ – contours (>0), increment 0.001.

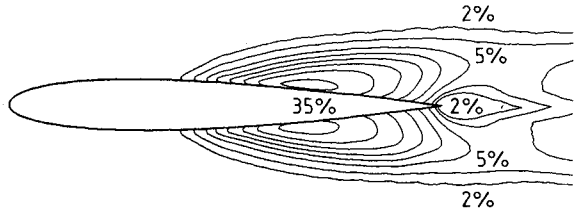

Fig. 2 NACA-0012 airfoil—contours of constant condensate mass fraction g/g_{max}, $\Phi_0 = 30\%$.

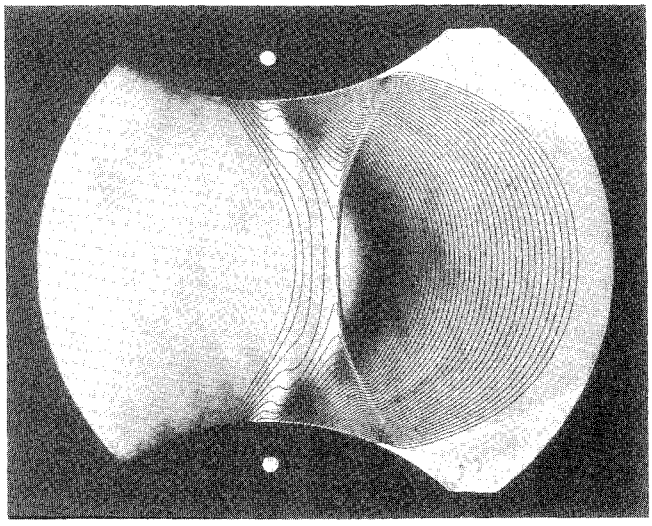

Fig. 3 Circular arc nozzle ($y^* = 60$ mm, $R^* = 100$ mm) – two-dimensional process, $\Phi_0 = 71.3\%$, M_f-contours ≥ 1, $\Delta M_f = 0.02$.

interesting contours of constant condensate mass fraction g/g_{max} are shown in Fig. 2. The difference in the contours of Figs. 1 and 2 results from the variable latent heat $L(T)$.

Nozzle Experiments

Figures 3 and 4 show typical Schlieren photographs of nozzle flows with homogeneous condensation. The experiments are compared with the calculated frozen Mach number contours. This Mach number is defined as the ratio of the local flow speed to the frozen speed of sound. In both nozzle flows, the reservoir conditions agree well with each other, and the cooling rates on the centerlines at the location where $M = 1$, relevant for the condensation onset, too. The differences are caused by two-dimensional effects from the wall curvatures. In Fig. 3 the condensation front attains the sonic line and acts on the oncoming flow.[20] In Fig. 4 the subsonic range obviously remains undisturbed. The high relative humidity causes the normal shock in the center followed by a local subsonic area. In Fig. 4 this area is extended across the whole height of the nozzle. Figures 3 and 4 show agreement between theory and experiment in the steady compression zones (light) as well as in the normal and oblique shocks. Both numerical results were based on the assumption of a solid condensate. For that case

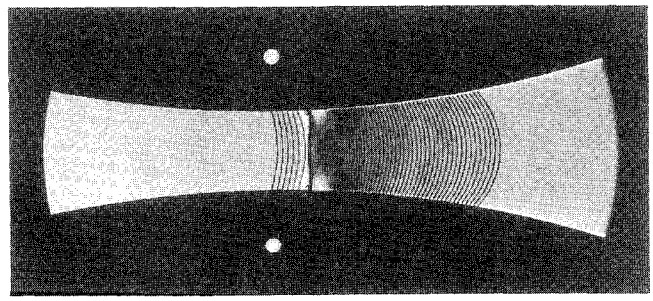

Fig. 4 Circular arc nozzle ($y^* = 15$ mm, $R^* = 400$ mm)-normal shock ahead of the main condensation region, $\Phi_0 = 73.4\%$, M_f-contours ≥ 1, $\Delta M_f = 0.02$.

a linearly decreasing function beginning from the known surface tension at the triple point and with the slope fitted to the experiments was assumed. The comparison of all nozzle experiments yields the following empirical relation for the surface tension

$$\sigma_\infty(T) = \begin{cases} T \geq 273.15 \text{ K} \\ (75.75 + 0.151\,(273.15 - T))\ 10^{-3} \text{ N/m} \\ (96.0 - 0.29\,(273.15 - T))\ 10^{-3} \text{ N/m} \\ T < 273.15 \text{ K} \end{cases} \tag{6}$$

The condensation coefficient of Eq. (3), important for the heat addition in the condensation zone, was found to be $\alpha \simeq 0.2 = \text{const}$.

For calculations based on the assumption of a liquid condensate, the experimental results of Peters and Paikert[21] were approximated by the following relation

$$\sigma_\infty(T) = \begin{cases} T \geq 249.4 \text{ K} \\ (76.1 + 0.155\,(273.15 - T))\ 10^{-3} \text{ N/m} \\ (1.131 - 3.709 \cdot 10^{-3} T)\ T^4 \cdot 10^{-10} \text{ N/m} \\ T < 249.4 \text{ K} \end{cases} \tag{7}$$

With $\alpha = \text{const}$, agreement with experiments could no longer be achieved. The following empirical relation was found

$$\alpha(T) = \begin{cases} 0.5 & T > 270 \text{ K} \\ 1 - 0.0125(T - 230) & 230 \text{ K} \leq T \leq 270 \text{ K} \\ 1 & T < 230 \text{ K} \end{cases} \tag{8}$$

Our result for liquid condensate and $\alpha \leq 1$ agrees with the experiments of Ref. 21. However, the agreement between experiment and numerical simulation cannot lead us to conclusions about the nature of the condensate—liquid or solid—in this low temperature range because of the simplifications in the classical theory for description of the homogeneous nucleation process; this question is still open. The calculations of all following numerical examples proceed from Eqs. (7) and (8), and the reservoir conditions of pressure and temperature are set up to $p_{01} = 10^5$ Pa and $T_{01} = 293.15$ K. The chord length of the airfoils—relevant for the time scale—are constant and equal 80 and 100 mm for the circular arc ($t = 0.1$) and the NACA-0012, respectively.

Circular Arc Airfoil—Experiments

The schlieren photograph in Fig. 5 shows a transonic flow with steady compression zones and the deformation of the rear shock, typical for small heat addition. All airfoil experi-

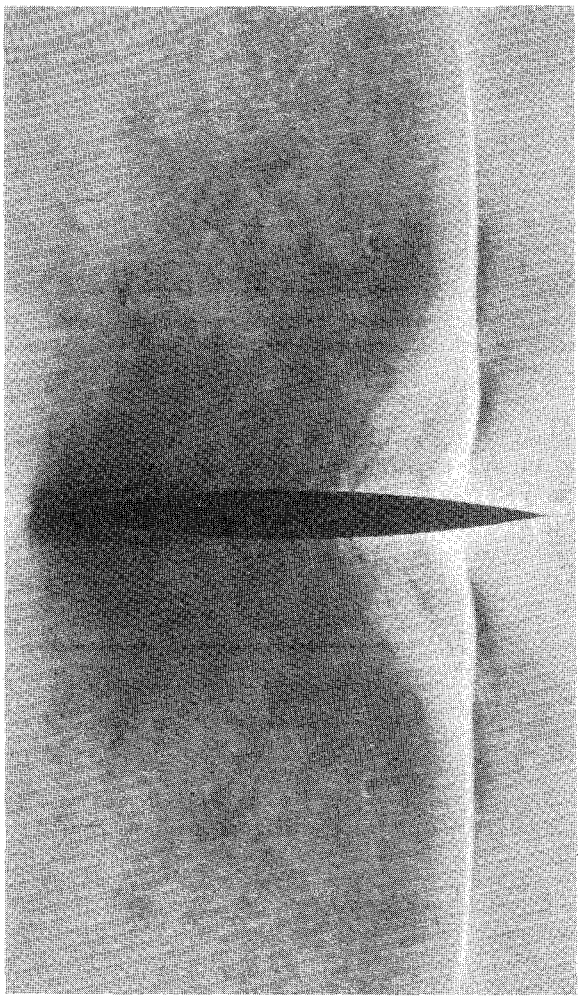

Fig. 5 Circular arc airfoil—weak compression by homogeneous condensation, $M_\infty = 0.791$, $\Phi_0 = 50\%$.

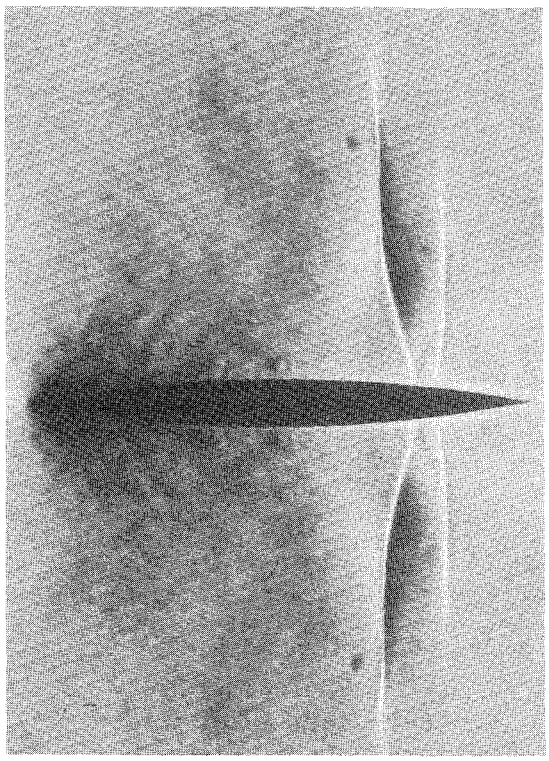

Fig. 6 Circular arc airfoil—λ—shock produced by heat addition, $M_\infty = 0.787$, $\Phi_0 = 57.1\%$.

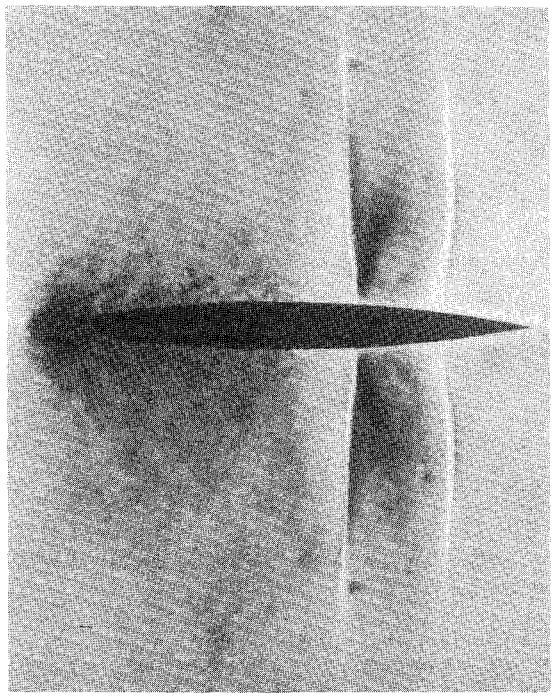

Fig. 7 Steady double shock system by supercritical heat addition, $M_\infty = 0.784$, $\Phi_0 = 64.1\%$.

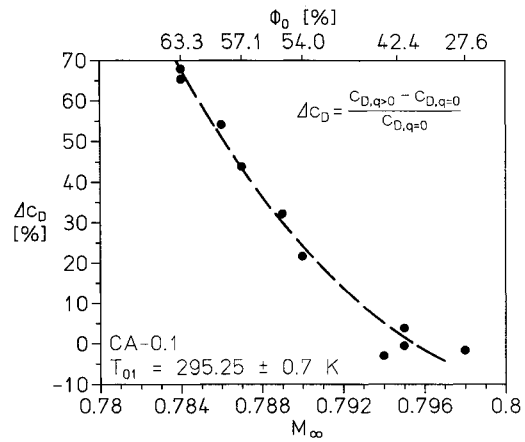

Fig. 8 Circular arc airfoil—flow with heat addition, pressure drag in a closed test section (height 170 mm)—experiment.

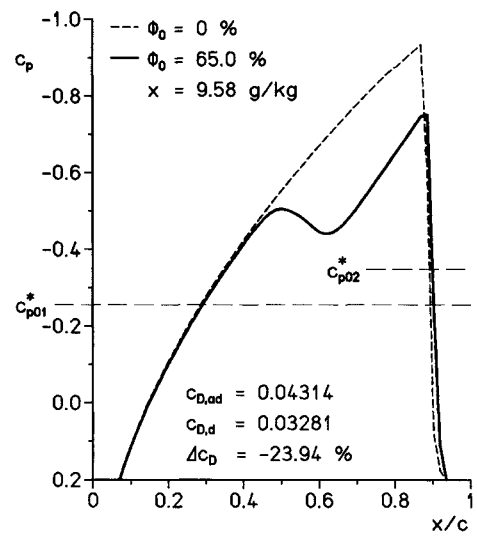

Fig. 9 Circular arc airfoil—theory, $M_{f,\infty} = 0.87$, static pressure distribution.

ments were made by means of half bodies, which were fixed on the bottom of the test section (atmospheric supply). For better illustration of the striking structures, the schlieren photographs were reflected to obtain airfoil presentations. For the development of the condensation process, the boundary layer influence can be reduced to its displacement effect, which does not alter the flow in principle.

In case of high onset Mach numbers, i.e., low relative humidities, the condensation process starts just ahead of the shock, and the onset front follows approximately an isotherm. When the heat addition is increased and the onset Mach number simultaneously decreased, the formation of an additional shock is observed (see Fig. 6). In the outer flowfield, two normal shocks follow each other, the Mach number between the two shocks is obviously $M<1$, and on the airfoil the heat addition is still steady. When the condensation onset shifts further to the sonic line, the heat addition becomes supercritical, and a steady double shock system develops (see Fig. 7). On the airfoil surface, the condensation onset is located upstream of the first shock. The possibility of such a double shock system already has been discussed by Zierep.[22]

From the pressure measurements, the drag coefficients for the adiabatic and diabatic case were calculated. The effects of skin friction and their variations due to the heat supply are not investigated. As an effect of heat addition, the pressure drag of an airfoil in a closed test section increases considerably (see Fig. 8). For the circular arc airfoil, the choking Mach number was $M_\infty=0.8$. Due to the experimental conditions, the reservoir properties Φ_0, x are not constant when varying the tunnel reference Mach number M_∞; they change inversely. The lower value M_∞ is related to the higher amount of heat and the higher relative humidity, i.e., lower condensation onset Mach number. This complex interaction and the test section interferences in adiabatic and diabatic flows do not permit general statements concerning the pressure drag behavior in free flow. They are provided by numerical simulations in the unbounded freestream.

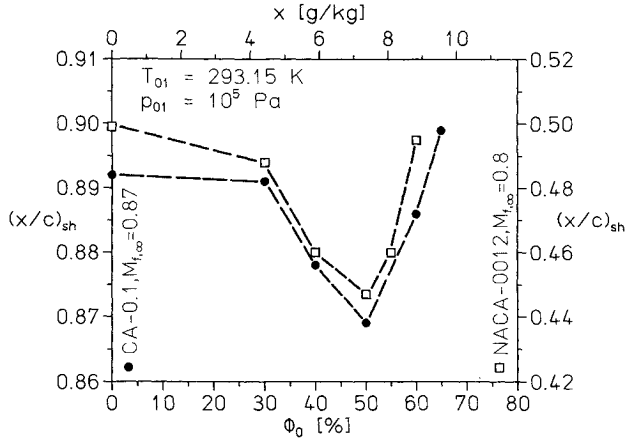

Fig. 10a Airfoils—theory, variation of relative humidity Φ_0, shift of the rear shock.

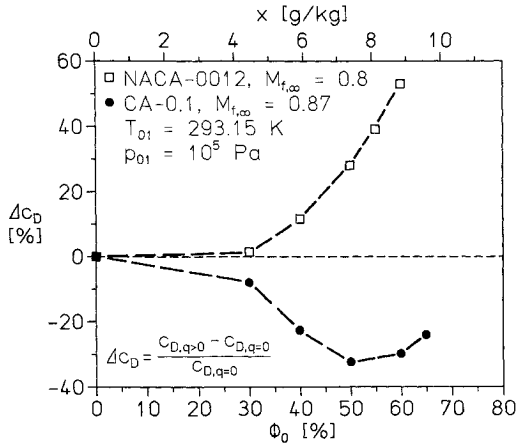

Fig. 10b Pressure drag coefficient by heat addition.

Circular Arc Airfoil—Theory

The theoretical results for a constant freestream Mach number $M_{f,\infty}=0.87$ are summarized in Figs. 9, 10a, and 10b. The critical values c_{p02}^* are related to the stagnation conditions after the heat supply. The decrease of the stagnation pressure yields a smaller critical pressure respective pressure coefficient. Whereas the shock in the experiment is clearly shifted towards the trailing edge, it now moves upstream at first and downstream again from $\Phi_0\approx 50\%$ upwards. At the beginning the influence of the compression is obviously prevailing in the local supersonic area. Finally for the lower onset Mach numbers near the thickness maximum of the airfoil, the expansion dominates and shifts the shock downstream (see Fig. 10a, left scale). Approximately the same behavior is established by the pressure drag (see Fig. 10b) and has to be expected for any other kind of heat addition in this area of the airfoil. It has a minimum at $\Phi_0\approx 50\%$, too. The theoretical results of Schnerr and Dohrmann[23] for the same airfoil are obtained with the assumption of a solid condensate. Using this assumption, the results of Figs. 10a and 10b are confirmed; the drag coefficients agree within 5%.

NACA-0012 Airfoil—Theory

The circular arc in the local supersonic range shows a roughly constant temperature gradient on the airfoil. However the NACA-0012 shows a distinct nonlinear acceleration near the leading edge, and downstream the gradients become smaller. This development affects the condensation onset. At a constant initial Mach number of $M_{f,\infty}=0.8$, without heat addition, the known shock position is at $x/c=0.5$. The increase of Φ_0 now demonstrates all 3 effects that cause the change of the pressure drag (see Fig. 11). Analogous to the circular arc airfoil, the pressure increases in the local supersonic region. The shock first is shifted forward more. At the same time, the droplets evaporate downstream of the shock. The reduced shock strength (pressure decrease) and the heat removal in the subsonic flow (pressure increase) altogether lead to a decrease of the static pressure in the rear section of the airfoil. Although a maximum forward shift of the shock is once again noted at $\Phi_0\approx 50\%$ (see Fig. 10a, right scale), the pressure drag continuously increases (see Fig. 10b). The up-

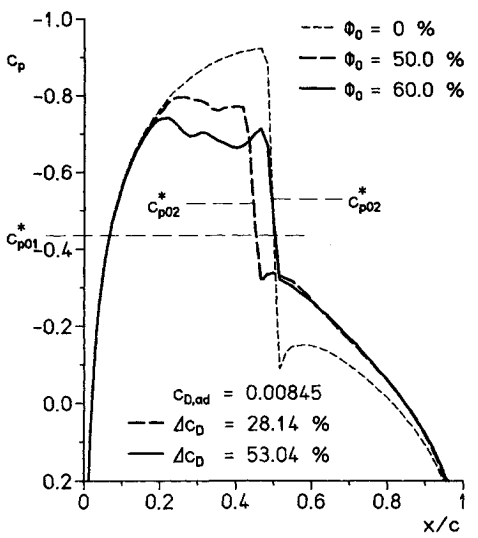

Fig. 11 NACA-0012 airfoil—theory, $M_{f,\infty}=0.8$, increase of relative humidity Φ_0.

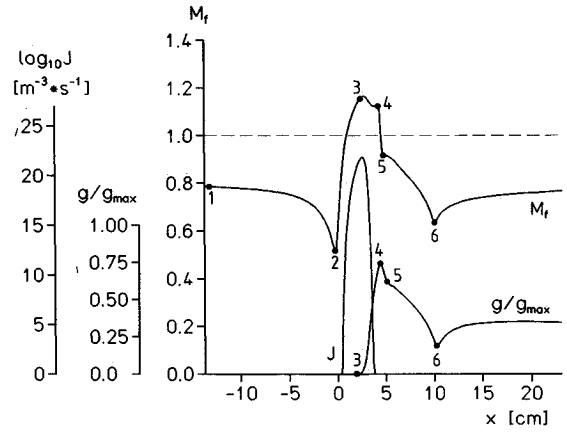

Fig. 12a NACA-0012 airfoil—theory, discussion along a streamline near the airfoil, $M_{f,\infty}=0.8$, $\Phi_0=50\%$, frozen Mach number M_f, nucleation rate J, condensate mass fraction g/g_{max}.

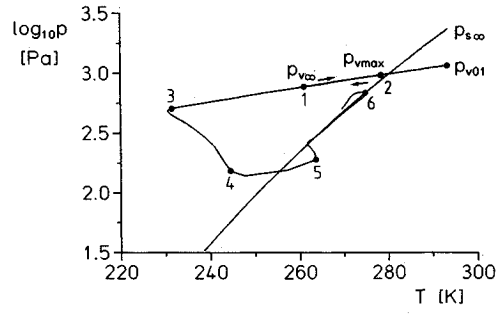

Fig. 12b Change of state in the phase diagram.

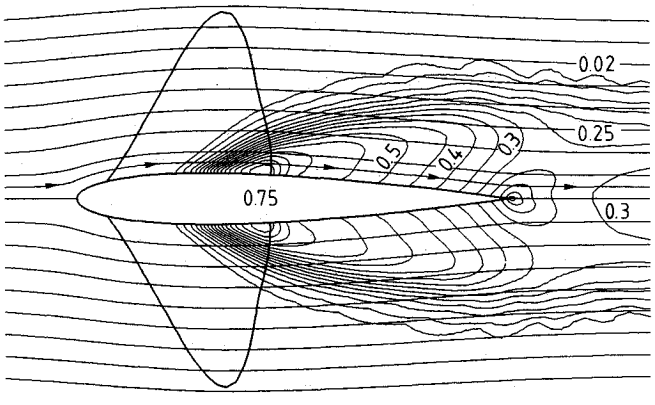

Fig. 12c Local supersonic region and g/g_{max} contours.

stream shock shift caused by low heat addition is noted for both airfoil series. It corresponds with the result in Ref. 8, obtained for a NACA-0012 at $M_{f,\infty}=0.8$ and an angle of attack of 2 deg.

For fixed stagnation conditions ($\Phi_0=50\%$), property changes near the airfoil and in the wake are shown by the results in Figs. 12a–12c. Figure 12a shows the Mach number distribution, the nucleation rate, and the condensate mass fraction along a streamline close to the airfoil surface. Near the airfoil the shock strength causes partial evaporation of the droplets. Approaching the rear stagnation area (6), the temperature arises further, and the condensate mass fraction decreases continuously. The following expansion causes a new increase of g/g_{max} since the freestream is evidently supersaturated. The latter fact is seen in Fig. 12b. In the p,T-diagram, the conditions along the same streamline and the equilibrium vapor pressure curve are plotted starting with the oncoming flow (1) and ending at the trailing edge (6). First the vapor

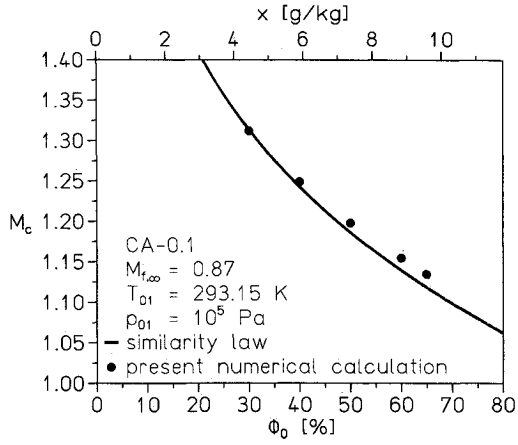

Fig. 13 Condensation onset on the circular arc airfoil, similarity law.[3,7]

component is isentropically compressed from (1) to (2) at the leading edge. Next follows the isentropic expansion up to the condensation onset at (3), followed by the nonequilibrium heat addition leading to (4). The normal shock is mapped on the line (4–5). As the preshock condition is located at the vapor pressure curve, the shock leads into the unsaturated state of the vapor phase, i.e., the droplets evaporate again. The further evaporation up to the trailing edge owing the increase of pressure is an equilibrium process along the vapor pressure curve to state (6). In Fig. 12c this fact is shown by means of contours of the condensate mass fraction. Streamlines and boundaries of the local supersonic area (sonic lines and shocks) are additionally plotted. Moreover Fig. 12c shows, that along streamlines on which local $M>1$ is obtained, condensation onset is no longer observed. Along these outer streamlines, only a reduced nucleation rate is noted, which vanishes again in the following compression.

Similarity Law

Fig. 13 shows the confirmation of the similarity law for the condensation onset Mach number M_c over the circular arc airfoil as a function of Φ_0 from Zierep and Lin[3] and Schnerr.[7] The numerical calculations with 5 different supply conditions prove the empirical results of Ref. 3 and 7 very well. The small deviations at higher values of Φ_0 can immediately be explained with the slight nonlinearity of the temperature rise over the airfoil. Zierep[24] furthermore specifies similarity laws for flows with heat addition over airfoils in all speed ranges. The constancy of the similarity parameters required there, however, presupposes the free choice of the heat source distribution. This assumption is not given for condensation processes due to the direct linkage of flow and heat supply.

Conclusions

Numerical simulation of transonic flows over airfoils including heat, supplied by homogeneous condensation of water vapor, including the classical theory of nucleation linked with the Euler equation is provided. It is founded that the pressure drag of an airfoil may be considerably increased or reduced, respectively. A pressure drag decrease is expected when the shock is located near the trailing edge. Otherwise the dominating pressure decrease in the subsonic flow behind the shock leads to a drag increase. For the condensation onset, the empirical similarity laws are well confirmed by the calculations. With the results obtained in this paper, a discussion of analogous variations of the lift coefficient is possible.

Acknowledgments

This work was partially supported by the Deutsche Forschungsgemeinschaft (DFG contract Zi 18-31) and the Klein, Schanzlin and Becker Stiftung (KSB contract No. 1111). The

authors are grateful to J. Zierep for suggesting this topic and the support in the course of realization of the project, and we would like to express our thanks to P. P. Wegener, Yale University, for helpful discussions during the preparation of this paper.

References

[1]Wegener, P. P., and Mack, L. M., "Condensation in Supersonic and Hypersonic Wind Tunnels," *Advances in Applied Mechanics,* Vol. 5, edited by Dryden/Kármán, 1958, Academic, New York, pp. 307–447.

[2]Oswatitsch, K., "Kondensationserscheinungen in Überschalldüsen," *Zeitschrift für Angewandte Mathematik und Mecanik,* Vol. 22, 1942, pp. 1–14.

[3]Zierep, J., and Lin, S., "Bestimmung des Kondensations-beginns bei der Entspannung feuchter Luft in Überschalldüsen," *Forschung im Ingenieurwesen,* Vol. 33, No. 6, 1967, pp. 169–172.

[4]Head, R., "Investigation in Spontaneous Condensation Phenomena," Ph.D. Thesis, Calif. Inst. of Technology, Pasadena, CA, 1949.

[5]Schmidt, B., "Schallnahe Profilumströmungen mit Kondensation," *Acta Mechanica,* Vol. 2, No. 3, 1966, pp. 194–208.

[6]Hiller, W. J., and Meier, G. E. A., "Grenzschichteffekte bei der Transsonischen Umströmung eines Symmetrischen Profils," MPI Göttingen, Bericht 9, 1977.

[7]Schnerr, G., "Homogene Kondensation in stationären transsonischen Strömungen durch Lavaldüsen und um Profile," Habilitationsschrift Universität (TH) Karlsruhe, Fakultät für Maschinenbau, 1986.

[8]Robinson, C. E., Bauer, R. C., and Nichols, R. H., "Estimating Water Vapor Condensation Effects for Transonic and Supersonic Flow Fields," AIAA Paper 85-5020, AIAA 3rd Applied Aerodynamics Conference, Colorado Springs, Colorado, Oct. 1985.

[9]Campbell, J. F., Chambers, J. R., and Rumsey, C. L., "Observation of Airplane Flow Fields by Natural Condensation," AIAA Paper 88-0191, AIAA 26th Aerospace Sciences Meeting, Reno, NV, Jan. 1989.

[10]Moheban, M., and Young, J. B., "A Time-Marching Method for the Calculation of Blade to Blade Non-equilibrium Wet Steam Flows in Turbine Cascades," Inst. Mechanical Engineering Conf. Publication, Computational Methods for Turbomachinery, Paper C 76184, Birmingham, 1984.

[11]Hall, R. M., "Onset of Condensation Effecst as Detected by Total Pressure Probes in the Langley 0.3-Meter Transonic Cryogenic Tunnel," NASA Technical Memorandum 80072, 1979.

[12]Hall, R. M., "Onset of Condensation Effects with an NACA 0012-64 Airfoil Tested in the Langley 0.3-meter Transonic Cryogenic Tunnel," NASA Technical Paper 1385, 1979.

[13]Koppenwallner, G., and Dankert, C., "An Experimental Study of Nitrogen Condensation in a Free Jet Expansion," *Rarefied Gas Dynamics, 11th Symp.,* edited by R. Compargue, Commissariat a L'Energie Atomique Paris, 1979, pp. 1107–1118.

[14]Wagner, B. and Düker, M., "Prediction of Condensation Onset and Growth in the European Transonic Wind Tunnel ETW," *AGARD-Conference Proceedings,* No. 348, pp. 13.1–13.11.

[15]Wegener, P. P., "Study of Experiments on Condensation of Nitrogen by Homogeneous Nucleation at States Modelling those of the National Transonic Facility," Final Report to the NASA Langley Research Center on Grant NSG-1612, 1980 (private communication).

[16]Wegener, P. P., "Nucleation of Nitrogen: Experiment and Theory," *Journal of Physical Chemistry,* Steinkopff-Verlag, Leipzig, Germany, Vol. 91, No. 10, 1987, pp. 2479–2481.

[17]Volmer, M., "Kinetik der Phasenbildung," Steinkopff-Verlag, Leipzig, 1939.

[18]Hill, Ph. G., "Condensation of Water Vapor during Supersonic Expansion in Nozzles," *Journal of Fluid Mechanics,* Vol. 25, No. 3, 1966, pp. 593–620.

[19]Eberle, A., "A New Flux Extrapolation Scheme Solving the Euler Equations for Arbitrary 3-D Geometry and Speed," Messerschmitt-Boelkow-Blohm, Munich, FRG, 1984.

[20]Schnerr, G., "2-D Transonic Flow with Energy Supply by Homogeneous Condensation: Onset Condition and 2-D Structure of Steady Laval Nozzle flow," *Experiments in Fluids,* Vol. 7, No. 3/4, 1989, pp. 145–156.

[21]Peters, F., and Paikert, B., "Nucleation and Growth Rates of Homogeneously Condensing Water Vapor in Argon From Shock Tube Experiments," *Experiments in Fluids,* (to be published).

[22]Zierep, J., "Schallnahe Strömungen mit Wärmezufuhr," *Acta Mechanica,* Vol. 8, No. 2, 1969, pp. 126–132.

[23]Schnerr, G., and Dohrmann, U., "Theoretical and Experimental Investigation of 2-D Diabatic Transonic and Supersonic Flow Fields," *Proceedings IUTAM Symposium Transsonicum III,* edited by J. Zierep and H. Oertel, Berlin-Heidelberg, FRG, 1989, pp. 125–135.

[24]Zierep, J., "Ähnlichkeitsgesetze für Profilumströmungen mit Wärmezufuhr," *Acta Mechanica,* Vol. 1, No. 1, 1965, pp. 60–70.